Analysis of Very-Low-Power E × B Discharge Seeded by Vacuum Arc Plasma

IEPC-2015-84／ISTS-2015-b-84

Presented at Joint Conference of 30th International Symposium on Space Technology and Science
34th International Electric Propulsion Conference and 6th Nano-satellite Symposium,
Hyogo-Kobe, Japan
July 4 – 10, 2015

Igal Kronhaus[1]
Technion – Israel Institute of Technology, Haifa, Technion City 3200003, Israel

Abstract: **An analysis of a very-low-power E × B discharge is performed. The efficiency of plasma generation is evaluated using simplified models and a fully kinetic two-dimensional particle-in-cell simulation. The concept of vacuum arc plasma seeding of an E × B discharge is introduced. For a 60 V ≈ 1 W E × B discharge, simulation results show that even at low seeding currents of < 3 mA significant increase in propellant utilization is obtained, from 0.2 up to 0.48. The seeding metal ions are accelerated significantly in the discharge chamber. Another advantage of the combined vacuum arc E × B discharge is improved ignition reliability.**

Nomenclature

A_{ch} = channel cross section area
B_r = radial magnetic field
C = proportional constant
d_{mc} = middle channel diameter
e = unit charge
E_z = axial electric field
f = proportional constant
h = channel width
I_{arc} = arc current
I_{Cu++} = Cu ions channel exit current
I_d = discharge current
$I_{i,Xe+}$ = Xe ions channel exit current
$J_{i,g}$ = propellant ions current density
k_i = propellant ionization rate
L = channel length
L_D = electron diffusion length
M = atom mass
$\dot{m}_g$ = propellant mass flow rate
$\dot{m}_{i,g}$ = propellant ion mass flow rate
n = plasma density
n_g = propellant gas density
$n_{i,g}$ = propellant ion density
$n_{i,m}$ = metal ion density
P_d = E × B discharge power
r = radial coordinate
T_e = electron temperature
U_d = discharge voltage
$\bar{v}_e$ = cell averaged electron velocity
v_g = propellant velocity
$v_{i,g}$ = propellant ion velocity
w_{Cu++} = metal plasma source rate
w_i = propellant ionization rate
z = axial coordinate
Z = ion charge state
α = Hall parameter
η_p = propellant utilization coefficient
λ_{ig} = propellant ionization mean free path
μ_B = Bohm's mobility
μ_{ez} = axial electron mobility
ν_e = electron collision frequency
σ_i = electron impact ionization cross section
τ_D = electron diffusion time
τ_i = electron gas ionization time
ω_{ce} = electron cyclotron frequency

[1] Assistant Professor, Department of Aerospace Engineering, kronhaus@tx.technion.ac.il

I. Introduction

HISTORICALLY Hall thrusters (HT) were designed to operate at power levels above 300 W. Scaling the same basic E × B discharge to lower operating power has proven to be difficult. Reports in the literature[1,2] indicate an electrical efficiency drop to 10 - 30 % at power levels below 100 W, mostly attributed to low propellant utilization.

As in other electrostatic thrusters the exhaust velocity is proportional to the square root of the discharge voltage, therefore, lower power regimes are accessible only by reducing the discharge current. A lower current, in turn, implies the use of a lower propellant mass flow rate. Finally, decreasing the mass flow rate results in an increased ionization mean free path length. Hence, two options are considered in order to improve propellant utilization: 1) channel extension; 2) increasing the initial residual plasma density.

Additionally, a Hall thruster discharge is controlled by wall recombination. Therefore, ion-wall interactions need to be considered as well.

As was shown in Ref. 3 simple extension of the channel provides only limited gains. The second method for improving propellant utilization, i.e., increasing the initial residual plasma density is not well established. One such approach is to mix a higher density plasma from a different source. A candidate for a seeding source is the vacuum-arc, an electrical discharge where plasma is directly generated from a solid metal cathode[4]. Over the past decades several investigations were carried out to characterize the metallic plume-gas interaction in low pressure gas. Most reported experimental work were conducted either with no magnetic field[5] or in axial magnetic field[6]. Except for an empirical study to develop a trigger mechanism for vacuum arcs[7], the author is not aware of attempts to study the interaction between metal vacuum arc plasma and ambient gas in an E × B discharge.

In section II of this paper we present a simplified analysis of a very-low-power E × B discharge chamber, focusing on major design parameters (geometry, mass flow rate, magnetic field, etc.). We introduce the concept of metallic plasma seeding by a vacuum arc, as a method to improve propellant utilization. In section III, simulation results of a very-low-power discharge chamber are presented. Ionization efficiency and related discharge parameters are analyzed and discussed.

II. Basic Principles of Very-Low-Power Seeded E × B Discharge-Chamber

A. Ionization Chamber Length

Ion production inside the chamber channel is done by collisional ionization. In this process, energetic electrons (typically with T_e ~ 10 - 20 eV) provide sufficient energy to ionize the atoms; in a HT most of the atoms are singly ionized. The distance an atom can travel before an ionization event is known as the ionization mean free path[8]:

$$\lambda_{ig} = \frac{v_g}{k_i n_e}, \tag{1}$$

where n_e is the number density of electrons, v_g is the mean velocity of the propellant atoms, and $k_i = \langle \sigma_i v_e \rangle$ is the ionization rate coefficient. It is useful to define a propellant utilization coefficient:

$$\eta_p = \frac{\dot{m}_{i,g}}{\dot{m}_g} \approx \frac{I_{i,g} M}{\dot{m}_g e}, \tag{2}$$

where $I_{i,g}$ is the propellant ion current at the exit of the thruster, M is the propellant atom mass, e is the unit charge, $\dot{m}_{i,g}$ is the propellant ion mass flow rate, and $\dot{m}_g$ is the propellant gas mass flow rate.

Assuming quasi-neutrality, the electron density can be written as:

$$n \equiv n_e \cong n_{i,g} = \frac{\eta_p \dot{m}_{i,g}}{M A_{ch} v_{i,g}}, \tag{3}$$

where n is the plasma number density, $n_{i,g}$ propellant ion number density, $v_{i,g}$ is the propellant ion speed. A_{ch} is the area crossed by the current. For the case of an annular channel with a middle channel diameter d_{mc} and a channel width h, we obtain:

$$A_{ch} = \pi d_{mc} h. \tag{4}$$

From Eqs. (1) - (3) the mean free path for propellant atom ionization is given by:

$$\lambda_{ig} = \frac{A_{ch}}{\eta_p \dot{m}_g} \frac{M v_g v_{i,g}}{k_i}. \tag{5}$$

Next we follow a standard analysis of electrical discharge kinetics[9]. The one dimensional continuity equations for the propellant atoms and ions are given by:

$$\frac{d(n_g v_g)}{dz} = -k_i n n_g, \tag{6}$$

$$\frac{d(n v_{i,g})}{dz} = k_i n n_g, \tag{7}$$

where z is the axial coordinate and n_g is the propellant number density. By assuming that both species move at constant velocities, Eq. (6) and Eq. (7) can be combined and integrated providing the following relation:

$$n v_{i,g} + n_g v_g = \frac{\dot{m}_g}{A_{ch} M}. \tag{8}$$

Replacing n_g in Eq. (6) with Eq. (8) we obtain an ODE of the first order in n:

$$v_{i,g}\frac{dn}{dz} = \frac{k_i \dot{m}_g n}{v_g A_{ch} M} - \frac{k_i v_{i,g} n^2}{v_g}. \tag{9}$$

By defining an initial and end-of-region propellant utilization coefficients η_{p0} and $\eta_{pL} \equiv \eta_p$ respectively, the solution to Eq. (9) is provided in the following form:

$$L = \lambda_{ig}\left(\eta_{pL} \ln\left|\frac{1-\frac{1}{\eta_{p0}}}{1-\frac{1}{\eta_{pL}}}\right|\right), \tag{10}$$

where L is the effective length of the discharge chamber.

Eq. (10) is plotted in Fig. 1. It can be easily recognized that, for a given L/λ_{ig}, increasing initial plasma density induces a large increase in the propellant utilization coefficient.

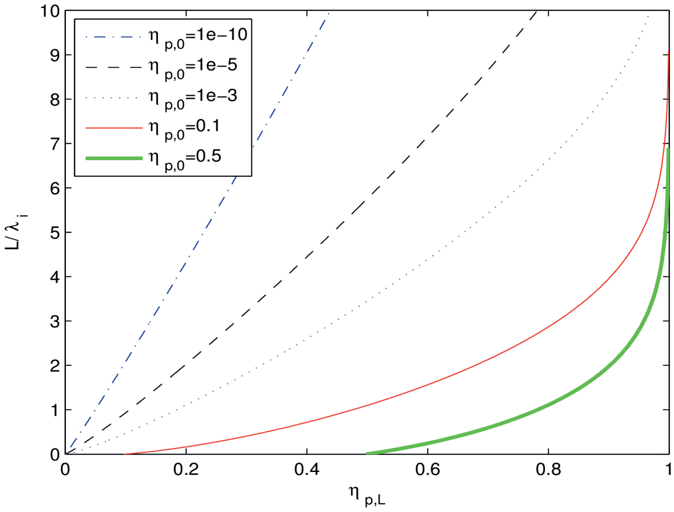

Figure 1. Ionization length dependence on propellant utilization factor as a function of initial plasma density.

B. Minimum Mass Flow Rate

By assuming a relatively high initial plasma density, one that is sufficient for $\eta_p \approx 1$ at $h = \lambda_{ig}$, Eq. (5) be can used to evaluate the condition for minimum mass flow rate:

$$\dot{m}_{g,min} > \frac{\pi d_{mc} M v_g v_{i,g}}{k_i}. \tag{11}$$

The ion velocity can be estimated from ion energy conservation:

$$v_{i,g} = \sqrt{\frac{2eU_d}{M}}, \tag{12}$$

where U_d is the discharge voltage.

As a test case for a very-low-power discharge chamber, we select a small annular channel with $d_m = 30\ \mathrm{mm}$ and $h = 1\ \mathrm{mm}$ (similar to the OEFT in Ref. 10). A $U_d = 60\ \mathrm{V}$ is selected to reduce the discharge power, taking into account that the electron-ion pair cost is about 40 eV.

In low power discharges, xenon propellant is preferred over other noble gases due to its relatively low ionization potential. Xenon can already be substantially ionized at low current density levels[11,2] as low as ~ 100 A/m^2. With an atom mass of $M = 2.2 \times 10^{-25}$ kg, the xenon ion velocity calculated according to Eq. (12) is $v_{i,g} = 9.3 \times 10^3\ \mathrm{m/s}$. Assuming near room temperature walls the propellant gas flow velocity[2] is $v_g \sim 100\ \mathrm{m/s}$. Similarly to HT, we estimate the electron temperature in the ionization region to be 10 – 20 eV, the ionization rate coefficient[11] is then $k_i(T_e = 16\ \mathrm{eV}) \approx 6.6 \times 10^{-14}\ \mathrm{m^3/s}$. Inserting these values to Eq. (11), the minimum value for the mass flow rate is $\dot{m}_{g,min} \approx 3 \times 10^{-7}\ \mathrm{kg/s}$. In this case, the corresponding xenon ion current at the exit is $I_{i,g} \approx 22\ \mathrm{mA}$.

C. Discharge Chamber Geometry and Magnetic Configuration

The discharge chamber can be operated either as a single stage or as a part of a double stage configuration, where it serves the function of a plasma source. In order to allow such design flexibility, the annular chamber walls are chosen to be conducting. For the case of a single stage, the walls are set at the cathode potential, and for the case of a double stage configuration, the walls are set to some intermediate potential.

The considered discharge chamber design includes two additional features: 1) the channel walls form part of the magnetic circuit; 2) the channel has a variable width, decreasing in size downstream towards the exit. These features allows several advantages: (a) generation of relatively high magnetic field near the exit due to the small gap; (b) increasing the gas density in the region of high magnetic induction; (c) the magnetic field lines intersect the wall perpendicularly, therefore electrons following the field lines are reflected back to the plasma bulk; (d) the width of the channel is increasing toward the ionization region, therefore, accommodating hot electrons with larger Larmor radii.

The magnetic field configuration follows that of a traditional Hall effect thruster, i.e., convex and increasing is strength towards the exit of the thruster. A schematic of the magnetic field lines and discharge chamber design is shown in Fig. 2.

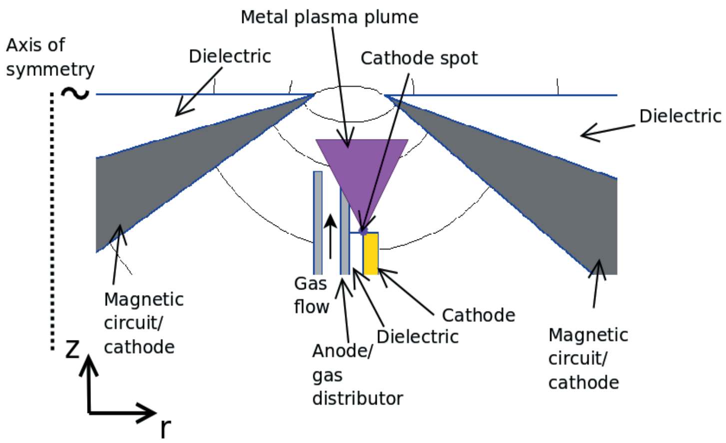

Figure 2. Schematic of a vary-low-power discharge chamber with vacuum arc seeding.

An estimate for the magnetic field strength can be obtained by assuming a balance of particles, between the electron-neutral ionization collision time τ_i and the electron diffusion time τ_D:

$$\frac{1}{k_i n_g} = \tau_i \approx \tau_D = \frac{L_D}{\mu_{ez} E_z}, \tag{13}$$

where E_z is the axial electric field, L_D is the electron diffusion length, and μ_{ez} is the axial mobility of electrons. It is well known that electron transport in an E × B discharge can depart significantly from classical mobility[12] therefore we use Bohm's mobility:

$$\mu_B = \frac{1}{\alpha B_r}, \tag{14}$$

where B_r is the radial component of the magnetic field and $\alpha = \omega_{ce}/\nu_e$ is the Hall parameter, defined as the ratio between the electron cyclotron frequency and the electron collision frequency. α is experimentally evaluated in the range 16 – 64[12,13]. Using Eq. (13) and Eq. (14) we obtain an approximate expression for the required magnetic field:

$$B_r \sim \frac{U_d}{\alpha L_D^2 k_i n_g}, \tag{15}$$

where $U_d \sim E_z L_D$. Setting $L_D = 2h = 2\ \mathrm{mm}$, $\alpha = 64$, $k_i = 6.6 \times 10^{-14}\ \mathrm{m^3/s}$, $U_d = 60\ \mathrm{V}$, and $n_g = 10^{20}\ \mathrm{m^{-3}}$ we obtain an estimate of $B_r \sim 0.03\ \mathrm{T}$.

D. Metallic Plasma Seeding

Assuming a fixed channel length, it is made clear from Fig. 1 that introducing significant plasma density near the gas outlet will enable higher fraction of propellant gas to be ionized. In this work a vacuum arc (VA) discharge is proposed to be used as a plasma seeding source. The VA is known to generate dense and fast moving plasma plumes ~ 10 km/s. For sufficiency low pressure < 10^{-4} mbar, as in our case, the VA plume interaction with the background gas can be neglected[4].

The VA plume is ejected from micrometer sized spots, also known as cathode spots, and follows a quasi-cosine distribution normal to the cathode surface $G(\theta)$, where θ being the angle to the discharge axis. The corresponding metal ion density is given by[14]:

$$n_{i,m} = \frac{C I_{arc} G(\theta)}{r^2}, \tag{16}$$

where the proportionality constant can be obtained by[14]:

$$C \approx \frac{f}{\pi Z e v_{i,m}} \approx 10^{13} \mathrm{A^{-1} m^{-1}}, \tag{17}$$

here *Z* is the ion charge state, $v_{i,m}$ is the metal ion velocity, and f is a known constant between 0.07 – 0.1.

The VA plume plasma density is proportional to the input power. Depending on the type of cathode material, experiments conducted on low current dc VA have shown that the minimal arc current is a few amperes[15], with typical discharge voltages in the range of 10 – 30 V. Therefore, at low power levels < 50 W, as considered in this work, the VA can only be used in a pulsed regime.

According to Eqs. (16) and (17) a $I_{arc} = 10\ \mathrm{A}$ at a distance of $L = 2h$ = 2 mm, will generate metallic plasma density of $n_{i,m} = 2.5 \times 10^{19}\ \mathrm{m^{-3}}$, which is about two orders of magnitude more than the E × B generated xenon plasma. Practically, therefore, only two combinations of VA and E × B discharge can be considered: 1) $I_{arc} f \gg I_d$; 2) $I_{arc} f \sim I_d$. For the first case the E × B discharge is used mainly as a triggering system for the VA. Similar ignition mechanisms were successfully used previously in industrial applications[7]. For the second case both the VA and E × B discharge contribute to plasma production and plasma acceleration. Next, we analyze the case of $I_{arc} f \sim I_d$ using numerical simulation.

III. Modeling and Results

A. Particle-In-Cell Numerical Model

A fully kinetic particle-in-cell simulation was used in the current investigation. Details about the program and the included physics can be found in Ref. 16. The model is two dimensional and axis-symmetric (all field quantities are assumed to be uniform in the azimuthal direction); the axial and radial coordinates are designated here as z and *r* respectively. Macro-particle velocity is tracked on all three dimensions.

A Poisson solver is used to obtain the electric potential in each electron time step, whereas the magnetic field is static. The domain boundary conditions are presented in Fig. 3. All field quantities are calculated on a rectilinear grid. Each cell volume is smaller than Debye sphere. The electron time step dt is chosen according to the ratio $\omega_p dt = 0.3$, where ω_p is the plasma frequency.

There are four macro-particle species in the simulation: electrons e^-, xenon neutrals Xe, single charged xenon ions Xe^+, and double charged copper ions Cu^{++}. Only collisions between electrons and xenon neutrals are modeled, these include: elastic, excitation, and single ionization. Excited atoms and ions are assumed to radiate and immediately return to the ground state. Xenon neutrals are accommodated on the walls and are emitted back with a half-Maxwellian distribution at the wall temperature 300 K. All other species are absorbed by the walls and boundaries, and therefore are effectively removed from the simulation. The number of real charged particles (electrons, ions) represented by a single macro-particle was set to 6.25×10^5. In a steady-state the average number of macro-particles present in the computational domain was ≈ 50,000.

The simulation represents true chamber geometry, dimensions, and includes real physical constants: mass, charge, and vacuum permittivity. In order to reduce the computational time heavy species are subcycled, i.e., advanced every 50 time steps for ions and 500 time steps for neutrals.

As shown in Fig. 3, the simulation domain includes three types of particle emitters: 1) An electron emitter simulating the cathode-neutralizer, where electrons are introduced according to a preset current; they are injected as a half-Maxwellian distribution at a temperature of 8 eV. When steady-state is achieved excess electrons return to the free space boundary to be deleted. 2) A xenon emitter simulating the anode/gas distributor, located upstream. Xenon particles are emitted as a half-Maxwellian distribution with a temperature of 0.05 eV. Emission is determined by a constant mass flow rate. 3) A volumetric plasma source introducing copper ions and electrons. Plasma is generated according to a predetermined rate in a narrow region (1 cell width) next to the gas distributor. This particle source simulates a broad cold beam of low density ions coming in from a distant VA source with an axial velocity of 10^4 m/s.

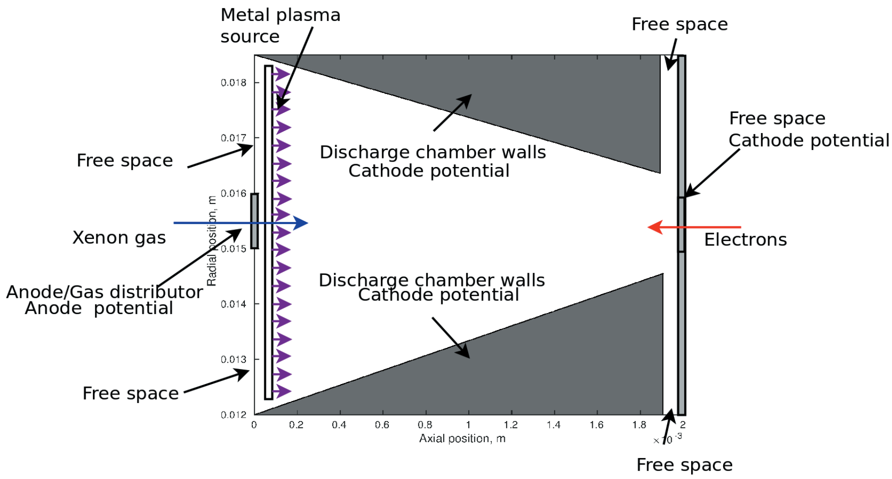

Figure 3. Schematic of the computational domain including boundary conditions and particle emitters.

The simulation starts with the introduction of xenon neutrals. This initial simulation runs until a steady-state distribution of xenon gas is established in the discharge chamber. Then, electrons and copper ions are added. The full species simulation is propagated for 100 μs. Calculation time is typically less than a day on a single core of an Intel Xeon 3.0 GHz machine (max frequency 3.6 GHz).

B. Simulation Results – Pure E × B Discharge

Several simulations were performed using different values of magnetic field strength. The numerical experiments have shown that above $B_r > 400$ G the discharge does not self-sustain. The highest η_p was achieved at $B_{r,max} \approx 300$ G. This magnetic field configuration was used in all subsequent simulations. Additionally, the channel length effectiveness in improving η_p was tested. No further improvement in η_p was found for $L > 2h$, therefore, $L = 2h$ was used in all subsequent simulations as well.

After we have selected the channel geometry and magnetic field, a parametric study of the discharge was carried out using different levels of steady-state discharge current magnitude. The steady-state parameters after 100 μs are shown in Table 1. As expected, the data indicates that the propellant utilization efficiency is increased with power. We note that in all cases the discharge current is dominated by the electronic component (over current regime).

Table 1. Steady-state discharge parameters, no metallic seeding, $\dot{m}_g = 3.8 \times 10^{-8}$ kg/s, at several discharge currents.

	Case 1	Case 2	Case 3	Case 4
I_d, mA	23.0	33.0	40.0	46.3
P_d, W	1.4	2.0	2.4	2.8
I_{Xe^+}, mA	5.4	8.5	10.5	13.2
η_p	0.20	0.30	0.38	0.48

The electron transport in the channel can be characterized by a Hall parameter α. Being fully kinetic, the simulation provides the entire distribution of macro-particles velocity. Therefore, the Hall parameter can be calculated as a ratio between azimuthal and axial electron velocity components:

$$\alpha|_{i,j} = \left|\frac{\bar{v}_{e\theta}}{\bar{v}_{ez}}\right|_{i,j} . \tag{18}$$

The calculation is performed in each cell by averaging the velocity components of all the macro-particles in that cell. The result is shown in Fig. 4. Although not uniformly distributed, a wide band of $\alpha \geq 64$ is observed between $z = 0.8 - 2.0$ mm. The value of α in the rest of the channel is suppressed to $\alpha \approx 16$.

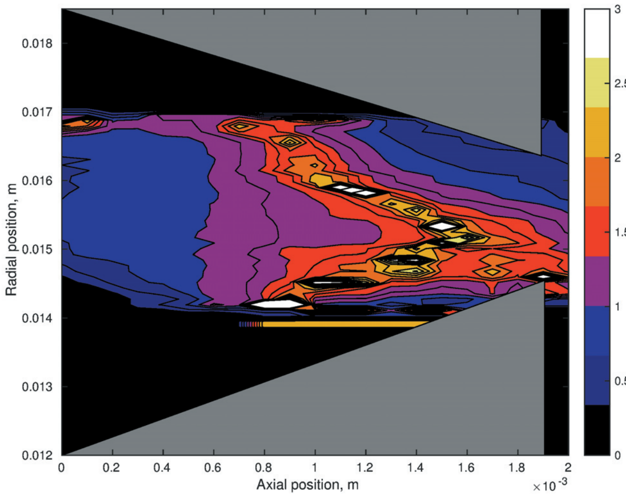

Figure 4. Hall parameter spatial distribution in log scale.

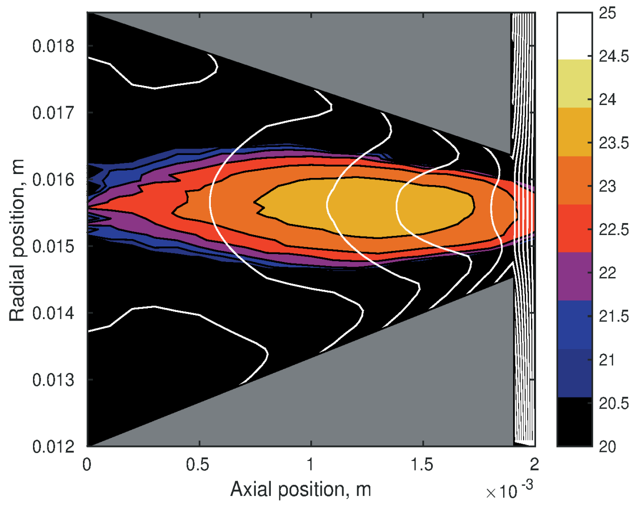

Figure 5. Ionization rate spatial distribution in log scale. Rate units in m^{-3}/s. Magnetic field lines are shown white.

Next, we present the spatial distribution of the ionization rate w_i. It is calculated according to: the mean electron velocity in each cell, the corresponding ionization cross section value, and the electron and propellant-gas densities:

$$w_i \,|_{i,j} = [n_g n_e \sigma_i(\bar{v}_e)\bar{v}_e]_{i,j} \,. \tag{19}$$

The result is shown in Fig. 5. We observe that the ionization is symmetric with respect to the mid channel. The region of high ion production rate of $w_i \approx 6.6 \times 10^{23}$ m^{-3}s^{-1} is spread over $z = 0.8 - 1.8$ mm which corresponds well with region of high Hall parameter.

Fig. 6 shows the radially-averaged normalized parameters of case 1 discharge (Table 1). The maximum plasma density is reached at $z \approx 1.5$ mm. Near the anode/gas distributor the electric field maintains a finite positive value that supports the electron current to the anode. Toward the exit, the electric field increases in strength. Electrons are heated in this region (their kinetic energy is indicated as KE_e) and provide effective ionization of the gas. The Xe^+ current density $J_{i,g}$ reaches a peak inside the channel and reduces toward the exit due to wall losses.

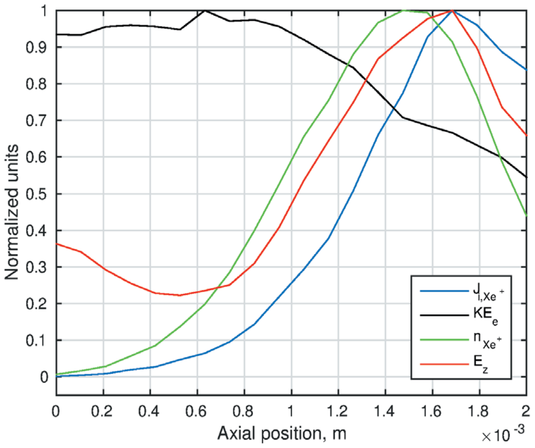

Figure 6. Radially-averaged normalized parameters of case 1 unseeded discharge.

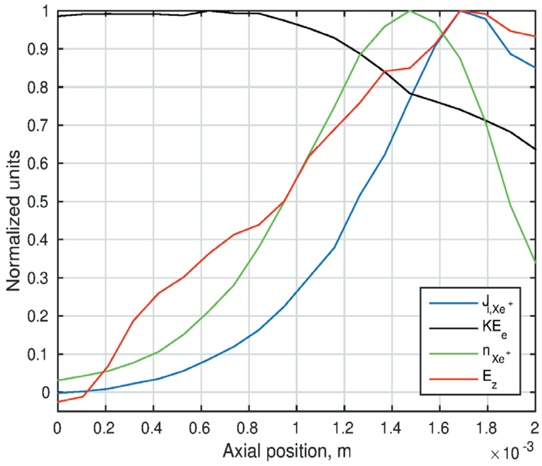

Figure 7. Radially-averaged normalized parameters of case 5 seeded discharge.

C. Simulation Results – E × B with Metallic Ion Seeding

Here, we introduce an additional plasma source next to the anode, as detailed in section III.A. This source injects double charged copper ions Cu^{++} as a cold beam with an axial velocity of 10 km/s. The accompanying metallic plasma electrons are injected with a thermal velocity at $T_e = 3$ eV. These parameters approximate a copper VA plume[4]. As representative cases, two source rates were simulated: $w_{\mathrm{Cu}^{++}} = 5 \times 10^{23}\ \mathrm{m}^{-3}\mathrm{s}^{-1}$ and $w_{\mathrm{Cu}^{++}} = 10^{24}\ \mathrm{m}^{-3}\mathrm{s}^{-1}$. Higher source rates were not attempted since the bulk plasma potential started to deviate from the the unseeded case, with a maximum difference of 5 V and 0.5 V for the higher and lower rates respectively.

In Fig. 7 we present the radially-averaged steady-state discharge parameters of case 5 (Table 2) with $I_d = 22.6$ mA and $w_{\mathrm{Cu}^{++}} = 5 \times 10^{23}\ \mathrm{m}^{-3}\mathrm{s}^{-1}$. The effect of the Cu^{++} seeding on Xe^+ production can be easily observed; about 5 % of the total xenon plasma density is generated immediately next to the anode, compared to < 1 % for the unseeded case. The increased initial plasma density enables large growth in the xenon ion current throughout the chamber. Here, the electric field is increasing towards the chamber exit in a nearly constant rate. We note that the electric field is negative close to the anode, and therefore impedes the electron flow to the anode.

The axial currents of both species along the discharge chamber length are presented in Fig. 8. In this case the Cu^{++} current is small $\approx 11\%$ the total ion current. Although the Cu^{++} ions are double charged and are about half in mass, due to their higher exit velocity they contribute a similar ratio ≈ 11 % to the total thrust. The discharge chamber therefore functions as a gridless vacuum-arc ion thruster, accelerating the metallic ions. This ion acceleration is demonstrated in Fig. 9 and Fig. 10 where the spatial distribution of xenon and copper ions are respectively presented.

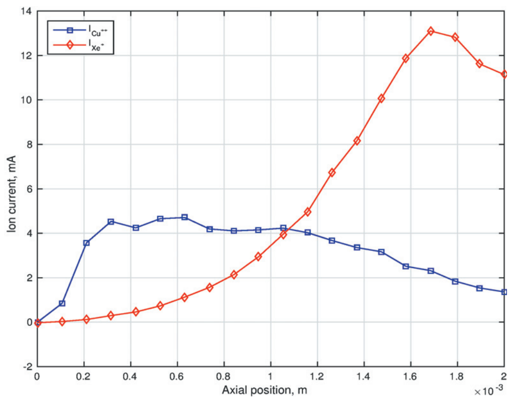

Figure 8. Radially-averaged currents versus position along the channel length.

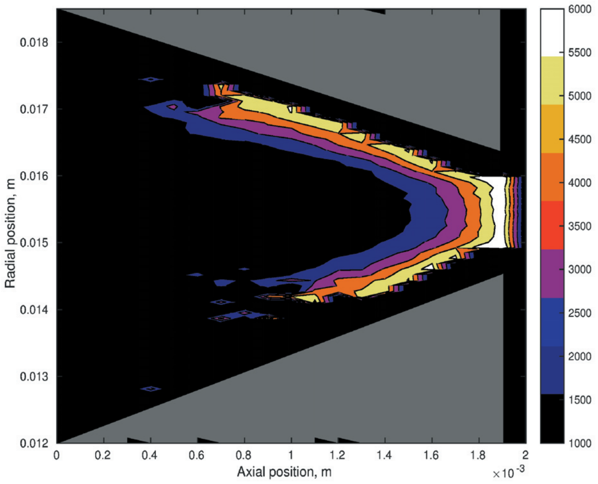

Figure 9. Spatial distribution of the axial velocity component of Xe$^+$ ions. Velocity units in m/s.

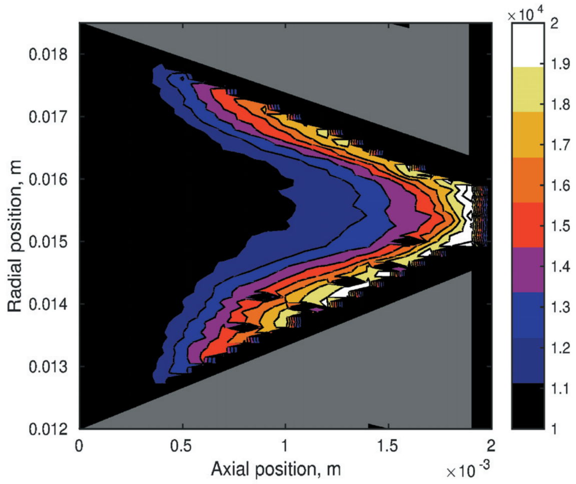

Figure 10. Spatial distribution of the axial velocity component of Cu^{++} ions. Velocity units in m/s.

A comparison between the steady-state parameters of seeded and unseeded cases is shown in Table 2. The most important fact observed is the large increase in η_p (calculated based on the Xe^+ current) when the metallic plasma seeding is employed, and the corresponding growth in total ion current at the chamber exit's $I_{\mathrm{Xe}^+} + I_{\mathrm{Cu}^{++}}$.

It is clear that gains in performance are only obtained during the operation of the VA. When the seeding is turned off, it only requires a few microseconds to revert back to the equilibrium state of the unseeded case.

Table 2. Steady-state discharge parameters, with seeding, $\dot{m}_g = 3.8 \times 10^{-8}$ kg/s.

	Case 1	Case 5	Case 6
I_d, mA	23.0	22.6	18.5
P_d, W	1.40	1.36	1.11
I_{Xe^+}, mA	5.4	11.4	13.0
$I_{Cu^{++}}$, mA	-	1.4	2.9
η_p	0.20	0.33	0.48

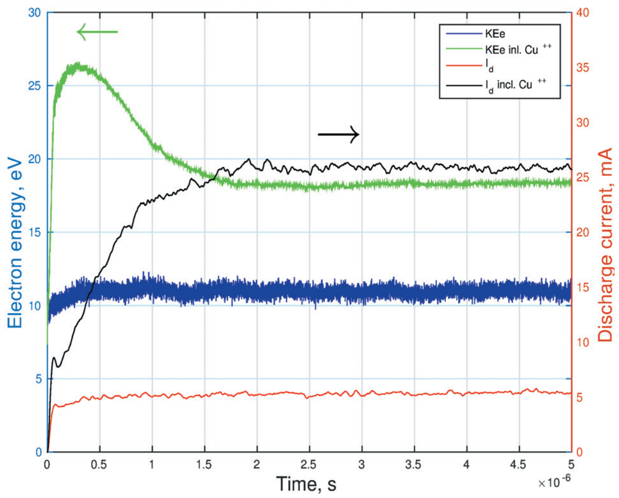

Figure 11. Evolution of electron kinetic energies and discharge currents after introduction of cathode electrons. Unseeded and seeded cases are shown (1 and 5 respectively).

Additional advantage of seeding is its assistance in discharge ignition. As shown in Fig. 11, when seeding is applied the discharge ignites immediately ~ 1 μs, conversely, without seeding the discharge does not ignite. In the later case a special procedure was required in order to ignite the discharge: either lowering the magnetic field strength or increasing the cathode electron temperature. Therefore, it can be concluded that the VA allows fast and easy ignition of the E × B discharge, and vice versa, the presence of E × B plasma assists VA ignition[7].

We note that the effects considered here are purely due to seeded plasma electrons, since the contribution of charge exchange and long-lived electronic excitations toward gas ionization were neglected. With the addition of these collisions, it is expected that the propellant utilization coefficient will further improve.

IV. Conclusion

In this paper we analyzed the performance of a very-low-power E × B discharge. Simple models were developed and a recommend discharge chamber design was provided. Particle-in-cell simulation of this chamber design have shown that it is capable of achieving propellant utilization factor of $\eta_p \approx 0.5$ at a discharge power of ≈ 3 W. To further improve its propellant utilization factor, the idea of vacuum arc seeding was introduced. The results show that with less than 1/5 of the total current, the VA seeding current facilitated achieving similar propellant utilization $\eta_p \approx 0.5$ at a discharge power as low as ≈ 1 W (not including the power required for the vacuum arc discharge).

Additionally, the combined discharge provides the following advantages:

1) reliable E × B discharge ignition, removing the need for complex ignition procedures such as lowering the magnetic field, therefore allowing the use of permanent magnets;
2) reliable ignition of the vacuum arc due to presence of the E x B plasma;
3) the discharge voltage provides acceleration of the vacuum arc plasma;
4) enables power/thrust control of an E x B discharge without valves or electromechanical actuators.

Future work will include regimes where the vacuum arc current dominates over the E × B discharge current.

References

[1]Ahedo, E., Lin, S., and Gallardo, J. M., "Scaling Down Hall Thrusters," 28th International Electric Propulsion Conference, Toulouse, France, 17–21 March, 2003, IEPC-2003-104.

[2]Shagayda, A. A., and Gorshkov, O. A., "Hall-Thruster Scaling Laws", *J. Prop. Power*, vol. 29, no. 2, pp. 466-474, 2013.

[3]Raitses, Y., Ashkenazy, J., and Guelman, M., "Propellant Utilization in Hall Thrusters," *J. Prop. Power*, vol. 14, no. 2, pp. 247–253, 1998.

[4]Anders, A., *Cathodic Arcs: From Fractal Spots to Energetic Condensation*, Springer, 2008.

[5]Grondona, D., Kelly, H., and Minotti, F., "Hydrodynamic Model for a Vacuum Arc Operated with Background Gas: Theory and Experimental Validation," *J. Appl. Phys.*, vol. 99, no. 4, p. 043304, 2006.

[6]Oks, E., and Anders, A., "Ion Species and Charge States of Vacuum Arc Plasma with Gas Feed and Longitudinal Magnetic Field." 24th International Symposium on Discharges and Electrical Insulation in Vacuum, Braunschweig, Germany, 30 August– 3 September, 2010.

[7]Nikolaev, A. G., Yushkov, G. Yu., Oks, E. M., MacGill, R. A., Dickinson, M. R., and Brown, I. G., "Vacuum Arc Trigger Systems Based on E × B Discharges," *Rev. Sci. Instrum.*, vol. 67, no. 9, pp. 3095–3098, 1996.

[8]Kim, V., "Main Physical Features and Processes Determining the Performance of Stationary Plasma Thrusters," *J. Prop. Power*, vol. 14, no. 5, pp. 736–743, 1998.

[9]Kapulkin, A. M., and Guelman, M., "Theoretical Modeling of Ionization Processes in Anode Cavity of CAMILA Hall Thruster." 31st International Electric Propulsion Conference, Ann Arbor, MI, 20–24 September, 2009, IEPC-2009-068.

[10]Kapulkin, A. M., Grishkevich, A. D., and Prisnyakov, V. F., "Outside Electric Field Thruster," *Space Technology*, vol. 15, no. 6, pp. 391–394, 1995.

[11]Morozov, A. I. and Savelyev, V. V., "Fundamentals of Stationary Plasma Thruster Theory," *Reviews of Plasma Physics*, vol. 21, pp. 203-390, 2000, Plenum Publishers.

[12]Meezan, N. B., Hargus W. A., and Cappelli, M. A., "Anomalous Electron Mobility in a Coaxial Hall Discharge Plasma," *Physical Review E*, vol. 63, no. 2, p. 26410, 2001.

[13]Kronhaus, I., Kapulkin, A. M., Balabanov, V., Rubanovich, M., Guelman, M., and Natan, B., "Investigation of Physical Processes in CAMILA Hall Thruster using Electrical Probes," *J. Phys. D: Appl. Phys.*, vol. 45, no. 17, p. 175203, 2012.

[14]Boxman, R. L., Sanders, D. M., and Martin, P. J., (Eds.), *Handbook of Vacuum Arc Science and Technology: Fundamentals and Applications,* Noyes Publication, 1995.

[15]Ding, C., and Yanabu, S., "Effect of Parallel Circuit Parameters on the Instability of a Low-Current Vacuum Arc," *IEEE Trans. Plasma Sci.*, vol. 31 , no. 5 , pp. 877 - 883 , 2003.

[16]Kronhaus, I., Kapulkin, A., Guelman M., and Natan, B., "Investigation of Two Discharge Configurations in the CAMILA Hall Thruster by the Particle-in-Cell Method," *Plasma Sources Sci. Technol.*, vol. 21, no. 3, p. 035005, 2012.